ACS APPLIED MATERIALS & INTERFACES

Letter

Cite This: ACS Appl. Mater. Interfaces 2018, 10, 7704−7708

www.acsami.org

Asymmetrically Curved Hyperbolic Metamaterial Structure with Gradient Thicknesses for Enhanced Directional Spontaneous Emission

Lu Wang,[†] Shilong Li,[‡,§] Biran Zhang,[†] Yuzhou Qin,[†] Ziao Tian,[†] Yangfu Fang,[†] Yonglei Li,[†] Zhaowei Liu,[§] and Yongfeng Mei*[,†]

[†]Department of Materials Science, State Key Laboratory of ASIC and Systems, Fudan University, Shanghai 200433, China

[‡]State Key Laboratory of Infrared Physics, Shanghai Institute of Technical Physics, Chinese Academy of Sciences, Shanghai 200083, China

[§]Department of Electrical and Computer Engineering, University of California, San Diego, California 92093, United States

Supporting Information

ABSTRACT: We demonstrate hyperbolic metamaterials (HMMs) on a curved surface for an efficient outcoupling of nonradiative modes, which lead to an enhanced spontaneous emission. Those high-wavevector plasmonic modes can propagate along the curved structure and emit into the far field, realizing a directional light emission with maximal fluorescent intensity. Detailed simulations disclose a high Purcell factor and a spatial power distribution in the curved HMM, which agrees with the experimental result. Our work presents remarkable enhancing capability in both the Purcell factor and emission intensity, which could suggest a unique structure design in metamaterials for potential application in, e.g., high-speed optical sensing and communications.

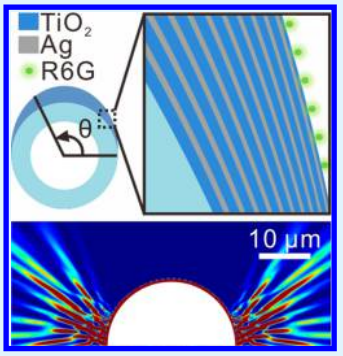

KEYWORDS: *hyperbolic metamaterial, spontaneous emission, outcoupling, directionality, Purcell factor, fluorescent intensity*

Hyperbolic metamaterials (HMMs), as one kind of artificial material featuring extraordinary electromagnetic properties because of its hyperbolic dispersion relationship, have recently attracted significant attention.[1,2] Unlike the elliptical dispersion of conventional materials, the hyperbolic dispersion results in a sharp increase in the photonic density of states (PDOS) and thus drastically alters the spontaneous emission rate of integrated light emitters.[3] Therefore, HMMs play a crucial role in both the fundamental and applied aspects of photonic devices for light emission and biosensing.[4−6] However, because HMMs are generally prepared in the form of a planar thin film, the spontaneous emission efficiency in the out-of-plane direction to the far field is extremely low because of the continuous translational symmetry of planar HMMs.[7] To overcome this obstacle, various nanopatterned structures have been utilized with planar HMMs for the far-field outcoupling.[8−10] In this Letter, we constructed a curved HMM with gradient thicknesses of metal/dielectric layers on top of a tubular structure without a continuous translational symmetry. The curved HMM features an asymmetric cross section with improved emission efficiency as well as directionality. Relevant calculations are performed to elucidate enhancement of the spontaneous emission rate, while enhancement of the emission directionality is verified by monitoring the emission intensity distribution based on angle-dependent microphotoluminescence (μ-PL) measurement, which matches well with the simulation results. The resulting HMM structure might be a promising candidate for the realization of a hyperlense,[11−13] liquid refractometers,[14] and a metamaterial-based light source.[15]

The HMMs used in this work consist of 20 stacked layers (10 periods) of metal Ag and dielectric TiO_2 deposited on top of a tapered glass capillary, which was obtained by pulling a heated glass capillary to reduce its diameter from around 1 μm to dozens of micrometers (see the Supporting Information, Part 1 and Figure S1). Both the TiO_2 and Ag layers were prepared by electron beam evaporation with thicknesses of 30 and 10 nm, respectively. On top of the uppermost Ag layer, an extra 10-nm-thick TiO_2 layer was deposited as a spacer layer to decrease the dye absorption. As shown in Figure 1a, the resulting HMM has a gradient in its thickness due to the directional deposition,[16] which meets our demands. Subsequently, the HMM-capped tapered glass capillary was dipped into the solution of Rhodamine 6G (R6G) with a concentration of 100 μM for 30 s and then dried in air. Figure 1b shows a scanning electron microscopy (SEM) image of the fabricated sample (cross-sectional view), where the boundary (dashed line) of the deposited HMM layer (w/HMMs) is clearly visible and the bottom part is without HMMs (w/o HMMs). The

Received: December 28, 2017
Accepted: February 13, 2018
Published: February 13, 2018

DOI: 10.1021/acsami.7b19721
ACS Appl. Mater. Interfaces 2018, 10, 7704−7708

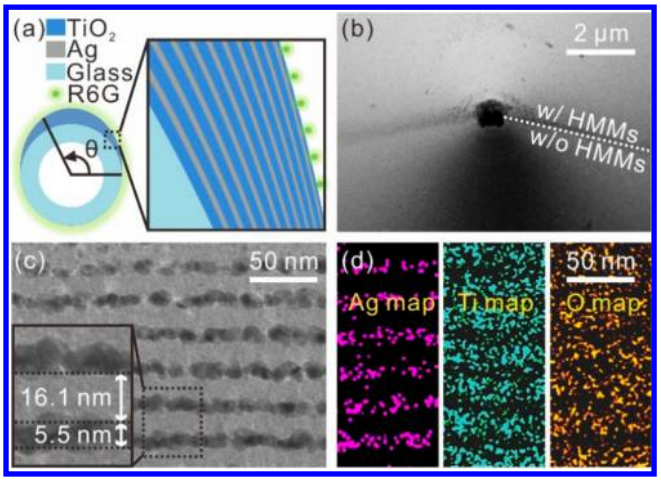

Figure 1. (a) Schematic configuration of the asymmetric HMM layer on a tapered glass capillary. The multilayers consist of Ag−TiO_2 stacks (the thicknesses of the Ag and TiO_2 layers are 10 and 30 nm, respectively, at θ = 90°). (b) SEM image of the fabricated sample at the smaller end from the top view. (c) STEM image of the stacked layers' cross section at θ = 30°. The bright area corresponds to TiO_2 and the dark to Ag. (d) Element mapping for the constituent materials (Ag, Ti, and O).

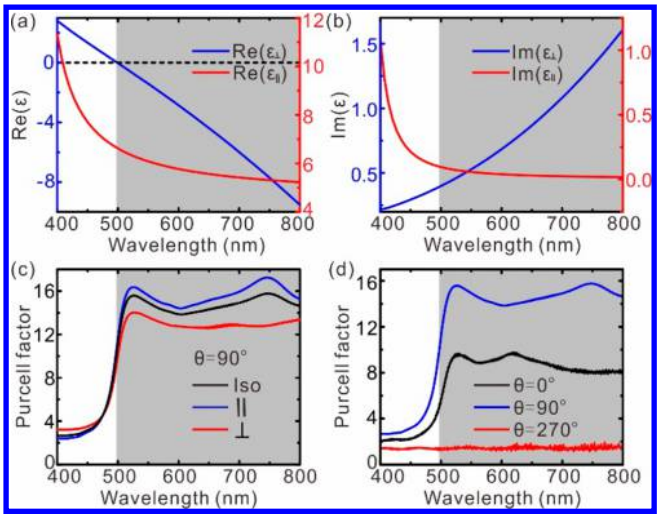

Figure 2. Calculated real (a) and imaginary (b) parts of the radial and tangential components of the effective permittivity for the fabricated TiO_2/Ag multilayer in a planar form. For a curved HMM layer on a tubular structure, the Purcell factor (c) for a dipole located at θ = 90° with the following orientations: parallel (∥), perpendicular (⊥), and isotropic. (d) Average Purcell factors at dipole locations of θ = 0°, 90°, and 270°.

cross-sectional details of the deposited multilayer structure were investigated by scanning transmission electron microscopy (STEM), and the focused-ion-beam milling process was adopted for the preparation of the sample's cross section. A typical STEM image of the cross section at θ = 30° is given in Figure 1c, showing the periodic multilayer structure, where θ is the angular position with respect to the parallel direction (see Figure 1a). It is noted that the thickness of one single layer at this position is nearly equal to half of the thickness of that at θ = 90°, as expected, while we can expect both better continuity and smoothness of the stacked layers at θ = 90°. Figure 1d shows the element mappings for Ag, Ti, and O, by which the structural periodicity and thickness are verified with good homogeneity.

The effective permittivity tensor for the fabricated dielectric/metal multilayer in the planar form can be calculated based on the effective media theory[17] as

$$\varepsilon_{\mathrm{p}}^{\mathrm{eff}} = \begin{bmatrix} \varepsilon_{\parallel} & 0 & 0 \\ 0 & \varepsilon_{\perp} & 0 \\ 0 & 0 & \varepsilon_{\parallel} \end{bmatrix} \tag{1}$$

$$\varepsilon_{\perp} = \frac{\varepsilon_{\mathrm{m}}\varepsilon_{\mathrm{d}}}{(1-p_{\mathrm{m}})\varepsilon_{\mathrm{m}} + p\varepsilon_{\mathrm{d}}} \tag{2}$$

$$\varepsilon_{\parallel} = p_{\mathrm{m}}\varepsilon_{\mathrm{m}} + (1-p_{\mathrm{m}})\varepsilon_{\mathrm{d}} \tag{3}$$

where ε_{d} and ε_{m} are the permittivities of dielectric TiO_2 and metal Ag, respectively, and $p_{\mathrm{m}} = t_{\mathrm{m}}/(t_{\mathrm{d}} + t_{\mathrm{m}})$ is the filling ratio of Ag. Here, the permittivity ε and thickness t of a single TiO_2 or Ag layer were determined by means of spectroscopic ellipsometry (see the Supporting Information, Part 1 and Figure S2), and the filling ratio p_{m} is designed to be 0.25 in order to have a better continuity of Ag layers. Parts a and b of Figure 2 show the calculated radial and tangential components of the effective permittivity tensor, respectively. It is clearly visible that a transition in the dispersion relationship of the dielectric/metal multilayer occurred from elliptical to hyperbolic as $\varepsilon_{\perp} < 0$ and $\varepsilon_{\parallel} > 0$, while the broad-band response and tunability can be engineered in the fabrication process.[18] A simple coordinate transformation gives the effective permittivity tensor for the resulting HMMs in the curved form:[19]

$$\varepsilon_{\mathrm{c}}^{\mathrm{eff}} = \begin{bmatrix} \varepsilon_{\perp}\cos^2\theta + \varepsilon_{\parallel}\sin^2\theta & (\varepsilon_{\perp}-\varepsilon_{\parallel})\sin\theta\cos\theta & 0 \\ (\varepsilon_{\perp}-\varepsilon_{\parallel})\sin\theta\cos\theta & \varepsilon_{\perp}\sin^2\theta + \varepsilon_{\parallel}\cos^2\theta & 0 \\ 0 & 0 & \varepsilon_{\parallel} \end{bmatrix} \tag{4}$$

which will be used in the simulation part of this work.

To estimate the spontaneous emission rate of a fluorescent molecule near the curved HMMs, the Purcell factor[20−22] was calculated based on the finite-element-method simulations (see the Supporting Information, Part 2). Here, a tapered glass capillary with a diameter of ∼20 μm and a wall thickness of ∼1 μm is considered, on top of which the dielectric/metal multilayer with a maximum thickness of ∼0.4 μm is applied. Considering the asymmetric feature of the curved HMMs, three Purcell factors in the cases of an electromagnetic dipole located at θ = 0°, 90°, and 270°, respectively, were calculated. The result for θ = 90° is shown in Figure 2c, where the dipole takes three orientations: parallel (∥), perpendicular (⊥), and isotropic with respect to the tangent. As can be clearly seen, the transition in the dispersion relationship results in an abrupt increase in the Purcell factor due to the PDOS enhancement as the wavelength increases over about 498 nm. Under the same circumstance, the dispersion transition dominates the Purcell effect; thus, a planar structure presents a value of the Purcell factor comparable to our proposed structure at θ = 90°. Moreover, by variation of the dipole location (Figure 2d), the Purcell factor can be tuned. Thus, one could utilize the curved HMMs to engineer the light−matter interaction when the Purcell effect is dominant.

The optical property of the tapered-glass-capillary-based asymmetrically curved HMMs was characterized by the μ-PL measurements. Owing to the cone-shaped feature of the

DOI: 10.1021/acsami.7b19721
ACS Appl. Mater. Interfaces 2018, 10, 7704−7708

capillary as shown in Figure 3a, characterizations were carried out as a function of the diameter. Here, a laser confocal μ-PL

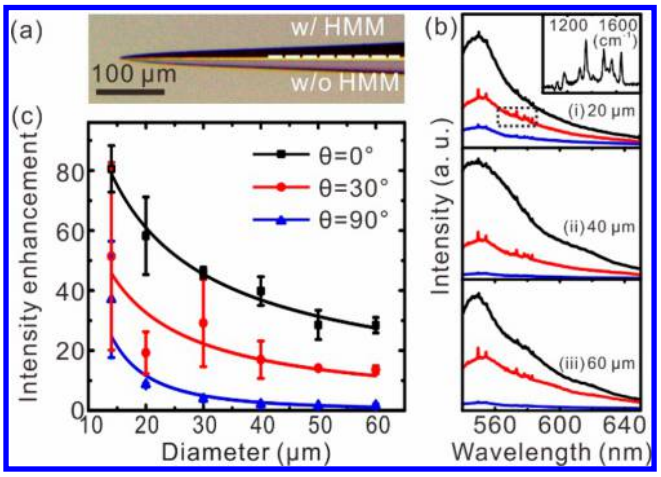

Figure 3. (a) Optical microscopy image of the tapered-glass-capillary-based asymmetrically curved HMMs. (b) μ-PL spectra of the resulting structure with diameters of ~20, ~40, and ~60 μm. The colored curves of black, red, and blue stand for the results from different excitation/collection angles θ of 0°, 30°, and 90°, respectively. The inset shows the Raman signal based on the data in the dashed box. (c) Experimental demonstration of the intensity enhancement with variable diameter and incident angle at an emission wavelength of 552 nm compared with that on the planar case.

setup was used to focus a 532 nm laser onto the surface of the HMMs to excite R6G molecules and then collect their broadband PL emission. The PL spectra of capillary samples with cross-sectional diameters D of ~20, ~40, and ~60 μm are depicted in Figure 3b. As can be seen, the PL intensity changes with the excitation and collection angle. In addition, enhanced Raman emissions of R6G molecules are achieved, especially at the collecting angle θ of 30°, as shown in the inset of Figure 3b(i). While θ is the angular position with respect to the thinnest point, the layer thickness at the angle θ of 30° induces a greatly enhanced light−matter interaction, where a large localized plasmonic enhancement is achieved because of the decreased continuity and smoothness of the deposited films.[23] In addition, the relationship between the cross-sectional diameter D and the emission enhancement is clearly seen in Figure 3c, where the ratio of the intensities at the emission wavelength of 552 nm of the curved-to-flat HMMs is shown. A stronger emission enhancement is obtained at a smaller cross-sectional diameter because of its larger curvature, where the intensity of the excited electromagnetic field increases, resulting in a better far-field light outcoupling.[24] In conclusion, these experimental results demonstrate both the enhancement and directionality of the emission due to the asymmetrically curved HMMs.

While the whispering-gallery mode resonances have been observed via the tapered fiber coupling method shown in Figure S3 (see also the Supporting Information, Part 3), they are absent in the μ-PL measurements because of the cone-shaped structure, which, by itself, cannot support any axial confinement for the emission light.[25] This nonresonance character ensures a wide-band emission enhancement. On the other hand, future work might be done on resonant curved HMMs by introducing an axial confinement via well-defined diameter variations.[26−28]

Moreover, to extract the emission directionality characteristics, a more detailed PL experiment was performed based on a capillary with a diameter of ~20 μm. In Figure 4a, the

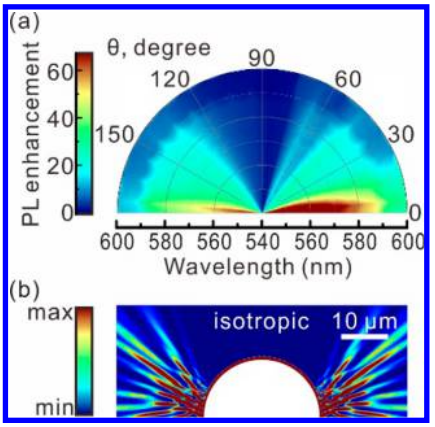

Figure 4. (a) Experimental demonstration of the intensity enhancement distribution at emission wavelengths of 540−600 nm by polar coordinates. The experiments were taken for the structure with a diameter of ~20 μm. (b) Theoretical result of the spatial power distribution (magnitude of the Poynting vector) at an emission wavelength of 552 nm. Dozens of dipoles with isotropic orientation were placed inside the HMM layer with consistent spacing between each one. The diameter was 20 μm.

experimental results of the intensity enhancement at emission wavelengths of 540−600 nm (depicted by the radial axis) demonstrate increased directionality and efficiency. The intensity enhancement was defined as the R6G molecules' emission on the resulting HMMs compared with that on planar HMMs. A maximum enhancement above 60 times can be achieved with the excitation and collection angles θ of about 0° and 180°. The intensity enhancement at θ = 0° and 180° results from the contributions of the outcoupling of nonradiative modes due to the notch where the thickness of the HMM layer is close to 0 nm gradually.

To further confirm this phenomenon, a simulation model with dozens of dipoles placed inside the HMM layer was completed for the stimulated emission. In Figure 4b, we present the power distribution of isotropic dipoles based on a curved structure with a diameter of 20 μm (see the Supporting Information, Part 4, for more details). The power distribution at an emission wavelength of 552 nm indicates propagation of the electromagnetic energy, which confirms the directional emission effect of using an asymmetrically curved structure. It is noticed that a number of waves travel inside the HMM layer until they hit its boundary,[29,30] while for the curved HMM layer, those modes with high wave vectors can be outcoupled to the free space thanks to the asymmetric structure-induced notch, which matches well with the experimental results of the intensity enhancement. Thus, as mentioned, for the proposed structure, it is feasible to realize a directional spontaneous emission enhancement while still embracing an excellent Purcell effect.

CONCLUSIONS

Asymmetrically curved HMMs exhibit enhancement for the spontaneous emission due to their unique outcoupling scheme for nonradiative waves. The intensity distribution detected through the μ-PL technique indicates enhancement of both the directionality and efficiency from the thickness-graded curved

DOI: 10.1021/acsami.7b19721
ACS Appl. Mater. Interfaces 2018, 10, 7704−7708

structure. Such curved HMMs, maintaining excellent property in the Purcell effect, can achieve a maximum intensity enhancement of about 80-fold for directional emission compared with planar HMMs. Our work offers an interesting design for HMMs to outcouple the plasmon modes for far-field emission, which could apply to other metamaterials and photonic structures for the required light−matter interaction.

■ ASSOCIATED CONTENT

Supporting Information

The Supporting Information is available free of charge on the ACS Publications website at DOI: 10.1021/acsami.7b19721.

Fabrication and optical properties, electromagnetic simulations of the Purcell effect, transmission measurements, electromagnetic simulations of the power distribution, and related experimental details (PDF)

■ AUTHOR INFORMATION

Corresponding Author

*E-mail: yfm@fudan.edu.cn.

ORCID

Yongfeng Mei: 0000-0002-3314-6108

Author Contributions

L.W., S.L., Z.L., and Y.M. conceived and designed the experiments. L.W. performed the experiments and simulations. Y.F. and Y.Q. guided the theoretical calculation. Z.T. and Y.L. contributed to the characterization. The manuscript was written through contributions of all authors. All authors have given approval to the final version of the manuscript.

Notes

The authors declare no competing financial interest.

■ ACKNOWLEDGMENTS

This work is supported by the Natural Science Foundation of China (Grants 61628401, U1632115, and 61728501), Science and Technology Commission of Shanghai Municipality (Grant 17JC1401700), National Key Technologies R&D Program of China (Grant 2015ZX02102-003), and Changjiang Young Scholars Program of China. Part of the experimental work has been carried out in Fudan Nanofabrication Laboratory. S.L. acknowledges financial support by the Office of China Postdoctoral Council (No. 32 Document of OCPC, 2017).

■ REFERENCES

(1) Poddubny, A.; Iorsh, I.; Belov, P.; Kivshar, Y. Hyperbolic Metamaterials. *Nat. Photonics* **2013**, *7*, 948−957.

(2) Ferrari, L.; Wu, C.; Lepage, D.; Zhang, X.; Liu, Z. W. Hyperbolic Metamaterials and Their Applications. *Prog. Quantum Electron.* **2015**, *40*, 1−40.

(3) Shalaginov, M. Y.; Vorobyov, V. V.; Liu, J.; Ferrera, M.; Akimov, A. V.; Lagutchev, A.; Smolyaninov, A. N.; Klimov, V. V.; Irudayaraj, J.; Kildishev, A. V.; Boltasseva, A.; Shalaev, V. M. Enhancement of Single-Photon Emission from Nitrogen-Vacancy Centers with TiN/(Al,Sc)N Hyperbolic Metamaterial. *Laser Photonics Rev.* **2015**, *9*, 120−127.

(4) Sreekanth, K. V.; Alapan, Y.; Elkabbash, M.; Ilker, E.; Hinczewski, M.; Gurkan, U. A.; De Luca, A.; Strangi, G. Extreme Sensitivity Biosensing Platform Based on Hyperbolic Metamaterials. *Nat. Mater.* **2016**, *15*, 621−627.

(5) Noginov, M. A.; Li, H.; Barnakov, Y. A.; Dryden, D.; Nataraj, G.; Zhu, G.; Bonner, C. E.; Mayy, M.; Jacob, Z.; Narimanov, E. E. Controlling Spontaneous Emission with Metamaterials. *Opt. Lett.* **2010**, *35*, 1863−1865.

(6) Kitur, J. K.; Gu, L.; Tumkur, T.; Bonner, C.; Noginov, M. A. Stimulated Emission of Surface Plasmons on Top of Metamaterials with Hyperbolic Dispersion. *ACS Photonics* **2015**, *2*, 1019−1024.

(7) Joannopoulos, J. D.; Johnson, S. G.; Winn, J. N.; Meade, R. D. *Photonic Crystals: Molding the Flow of Light*; Princeton University Press, 2008.

(8) Krishnamoorthy, H. N. S.; Jacob, Z.; Narimanov, E.; Kretzschmar, I.; Menon, V. M. Topological Transitions in Metamaterials. *Science* **2012**, *336*, 205−209.

(9) Lu, D.; Kan, J. J.; Fullerton, E. E.; Liu, Z. W. Enhancing Spontaneous Emission Rates of Molecules Using Nanopatterned Multilayer Hyperbolic Metamaterials. *Nat. Nanotechnol.* **2014**, *9*, 48−53.

(10) Sreekanth, K. V.; Krishna, K. H.; De Luca, A.; Strangi, G. Large Spontaneous Emission Rate Enhancement in Grating Coupled Hyperbolic Metamaterials. *Sci. Rep.* **2015**, *4*, 6340.

(11) Liu, Z. W.; Lee, H.; Xiong, Y.; Sun, C.; Zhang, X. Far-Field Optical Hyperlens Magnifying Sub-Diffraction-Limited Objects. *Science* **2007**, *315*, 1686.

(12) Lu, D.; Liu, Z. W. Hyperlenses and Metalenses for Far-Field Super-Resolution Imaging. *Nat. Commun.* **2012**, *3*, 1205.

(13) Jacob, Z.; Alekseyev, L. V.; Narimanov, E. Optical Hyperlens: Far-Field Imaging Beyond the Diffraction Limit. *Opt. Express* **2006**, *14*, 8247−8256.

(14) Tang, S. W.; Fang, Y. F.; Liu, Z. W.; Zhou, L.; Mei, Y. F. Tubular Optical Microcavities of Indefinite Medium for Sensitive Liquid Refractometers. *Lab Chip* **2016**, *16*, 182−187.

(15) Kildishev, A. V.; Boltasseva, A.; Shalaev, V. M. Planar Photonics with Metasurfaces. *Science* **2013**, *339*, 1232009.

(16) Hawkeye, M. M.; Brett, M. J. Glancing Angle Deposition: Fabrication, Properties, and Applications of Micro-and Nanostructured Thin Films. *J. Vac. Sci. Technol., A* **2007**, *25*, 1317−1335.

(17) Poddubny, A. N.; Belov, P. A.; Kivshar, Y. S. Spontaneous Radiation of a Finite-Size Dipole Emitter in Hyperbolic Media. *Phys. Rev. A: At., Mol., Opt. Phys.* **2011**, *84*, 023807.

(18) Morgan, F.; Murphy, A.; Hendren, W.; Wurtz, G.; Pollard, R. J. In Situ Ellipsometric Monitoring of Gold Nanorod Metamaterials Growth. *ACS Appl. Mater. Interfaces* **2017**, *9*, 17379−17386.

(19) Smith, E. J.; Liu, Z. W.; Mei, Y. F.; Schmidt, O. G. Combined Surface Plasmon and Classical Waveguiding through Metamaterial Fiber Design. *Nano Lett.* **2010**, *10*, 1−5.

(20) Purcell, E. M. Spontaneous Emission Probabilities at Radio Frequencies. *NATO ASI Ser., Ser. B* **1995**, *340*, 839.

(21) Liaw, J.-W. Local-Field Enhancement and Quantum Yield of Metallic Dimer. *Jpn. J. Appl. Phys.* **2007**, *46*, 5373−5378.

(22) Novotny, L.; Hecht, B. *Principles of Nano-Optics*; Cambridge University Press, 2012.

(23) Lin, X. Y.; Fang, Y. F.; Zhu, L. J.; Zhang, J.; Huang, G. S.; Wang, J.; Mei, Y. F. Self-Rolling of Oxide Nanomembranes and Resonance Coupling in Tubular Optical Microcavity. *Adv. Opt. Mater.* **2016**, *4*, 936−942.

(24) Huang, G. S.; Mei, Y. F. Electromagnetic Wave Propagation in a Rolled-up Tubular Microcavity. *J. Mater. Chem. C* **2017**, *5*, 2758−2770.

(25) Sumetsky, M. Mode Localization and the Q-Factor of a Cylindrical Microresonator. *Opt. Lett.* **2010**, *35*, 2385−2387.

(26) Wang, J.; Zhan, T. R.; Huang, G. S.; Cui, X. G.; Hu, X. H.; Mei, Y. F. Tubular Oxide Microcavity with High-Index-Contrast Walls: Mie Scattering Theory and 3D Confinement of Resonant Modes. *Opt. Express* **2012**, *20*, 18555−18567.

(27) Fang, Y. F.; Lin, X. Y.; Tang, S. W.; Xu, B. R.; Wang, J.; Mei, Y. F. Temperature-Dependent Optical Resonance in a Thin-Walled Tubular Oxide Microcavity. *Prog. Nat. Sci.* **2017**, *27*, 498−502.

(28) Bolãnos Quiñones, V. A.; Ma, L. B.; Li, S. L.; Jorgensen, M.; Kiravittaya, S.; Schmidt, O. G. Enhanced Optical Axial Confinement in Asymmetric Microtube Cavities Rolled Up from Circular-Shaped Nanomembranes. *Opt. Lett.* **2012**, *37*, 4284−4286.

(29) West, P. R.; Kinsey, N.; Ferrera, M.; Kildishev, A. V.; Shalaev, V. M.; Boltasseva, A. Adiabatically Tapered Hyperbolic Metamaterials for Dispersion Control of High-k Waves. *Nano Lett.* **2015**, *15*, 498−505.
(30) Ferrari, L.; Smalley, J. S. T.; Fainman, Y.; Liu, Z. W. Hyperbolic Metamaterials for Dispersion-Assisted Directional Light Emission. *Nanoscale* **2017**, *9*, 9034−9048.

DOI: 10.1021/acsami.7b19721
ACS Appl. Mater. Interfaces 2018, 10, 7704−7708